Theoretical Computer Science 406 (2008) 160–170

Contents lists available at ScienceDirect

Theoretical Computer Science

journal homepage: www.elsevier.com/locate/tcs

On image reconstruction algorithms for binary electromagnetic geotomography

Rafal Zdunek *

Institute of Telecommunications, Teleinformatics and Acoustics, Wroclaw University of Technology, Wybrzeze Wyspianskiego 27, 50–370 Wroclaw, Poland

ARTICLE INFO

Keywords:
Binary electromagnetic geotomography
Mean-field annealing
Projected gradient
Limited-data tomography

ABSTRACT

In this paper we discuss the selected image reconstruction methods of binary tomography in the context of their application to geophysical imaging. We restrict our considerations to a discrete version of high-frequency electromagnetic geotomography, which we label as Binary Electromagnetic Geotomography (BEG). Basically, such an imaging technique may be applied to detect subsurface anomalies (air-filled voids) whose attenuation coefficient is very low (nearly zero-value) and considerably different from that for the background. The assumption for a binary representation of the image to be reconstructed substantially relaxes image reconstruction problems related to ill-posedness that comes from an intrinsic limitation of an angular range of projections. We test two algorithms for binary tomography, where the penalty term is based on the Markov Random Field (MRF) model. The mean-field reference distribution and mean-field annealing are applied to estimate the global maximizer of the Gibbs–Boltzmann distribution associated with the objective function. We also apply the projected gradient algorithm that uses a binary steering. Very efficient implementations of the algorithms are also given. The numerical results are presented for noise-free, noisy, and real data.

1. Introduction

In geophysical prospecting [46], tomographic imaging is widely used for mapping the interior structure of the ground. This technique is also very helpful in localization and characterization of subsurface anomalies, such as cracks, cavities, tunnels or voids, which may result from lithological characteristics or human activities [22,42].

In this paper, our considerations are focused on the technique that is intended to visualize subsurface air-filled voids that may occur due to the collapse of inactive coal mines. Detection of such anomalies may be performed with many measurement configurations, e.g. near-surface measurements, vertical profiling or sectioning. In geophysical tomographic imaging, which is mainly related to the sectioning, the cross-section between boreholes is surveyed. An example of this technique (also known as borehole or cross-hole tomography) is seismic tomography [8,16,22,48]. It is potentially useful when there is a marked contrast in the properties of the ground, and therefore, it is commonly-used for detection of subsurface anomalies. However, there are some explorations in which seismic methods have very limited applications. Seismic waves excite ground tremors that may be very dangerous for the objects located in the region with mining damage. For such explorations, electromagnetic methods are much more helpful. Air-filled anomalies have considerably different electric properties from that for the background (sedimentary rocks), and hence, they can be easily detected with electromagnetic probings between boreholes.

The borehole tomographic technique in which electromagnetic waves are used is known in the literature [15,42] as Electromagnetic Geotomography (EG). The geometry of interest in EG is cross-borehole scanning. The data is gathered along

* Tel.: +48 71 320 3215; fax: +48 71 322 3664.
E-mail address: zdunek@brain.riken.jp.

0304-3975/$ – see front matter © 2008 Elsevier B.V. All rights reserved.
doi:10.1016/j.tcs.2008.06.007

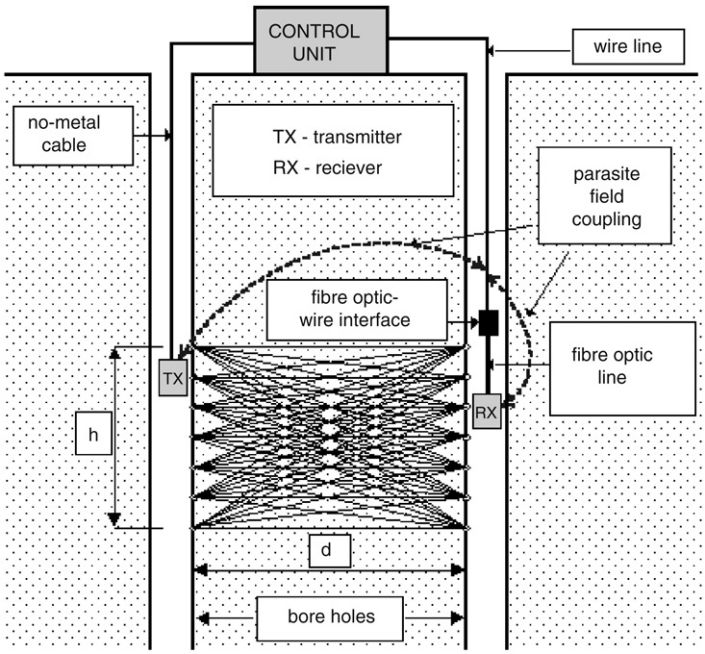

Fig. 1. Schematic diagram of the measurement system.

multiple ray-paths that link the positions of the transmitting probe (transmitter) and the receiving probe (receiver). This is schematically depicted in Fig. 1. The region of interest is a $h \times d$ rectangular, where h is the height of the horizontal layer of interest, and d is the distance between the boreholes.

The electrical properties of the surveyed medium along each ray-path affect the transmission properties of the electromagnetic waves propagated along that ray-path. Therefore, the measured data carries the information about the unknown geological structure. Our study is based on an absorption model that describes the attenuation of electromagnetic waves along the straight-line ray-path, and therefore, this model can be expressed in terms of the Radon transform. The "straight-ray" approximation neglects the effects of reflection, refraction and diffraction, and it is justified provided that the electromagnetic waves of high frequencies are used [15,40,51]. An inversion of the model yields an image of spatial distribution of electromagnetic wave attenuation coefficient in the surveyed area.

Many algorithms [53,57,59] have been developed to solve the inverse problem in borehole tomography. The Algebraic Reconstruction Technique (ART), Simultaneous Iterative Reconstruction Technique (SIRT), or various implementations of Conjugate Gradient (CG) methods (e.g. CGLS, LSQR) are examples of iterative methods that are commonly-used in geophysical imaging. The direct inversion algorithms that usually involve the Singular Value Decomposition (SVD) are also widely applied for this purpose.

The above-mentioned algorithms give the least-squares approximations of the true solution. For noise-free data (consistent case), the approximations are convergent to the least-squares solution of minimal l_2-norm. In practice, any perturbations in measurements introduce inconsistency to the model, and hence, the methods may give only approximations that are in a certain, more or less controllable distance to the minimal-norm least-square solution.

In borehole imaging, due to the intrinsic limitation of an angular range of the ray-paths, the model can be treated as underdetermined, and consequently an ill-posed problem has to be solved. As a result, reconstructed images are spoilt with vertical smeared structures. These effects, which are often called "ghosts", have been widely discussed in the literature [2,8,16,32]. Koltracht et al. [32] proved that for borehole tomography, the nullspace of the forward projection operator is non-trivial, which implies that the inversion is non-unique, and the minimal-norm least-square solution may not be the true solution. In many borehole imaging techniques, the ambiguity of inversion and related artifacts are reduced by suitable regularization that stabilizes the solution or improves it with some prior information. However, efficient regularization of the solution is a very challenging task, and it requires careful treatment of the prior information. In many cases, the prior knowledge on the solution is limited, e.g. only to a degree of smoothness or sparsity. In EG, the constraints on boundary values, especially for the lower bound (non-negativity), can be also imposed. All the assumptions obviously improve the solution, however, something more can be still done.

The air-filled voids have considerably different electrical parameters than that for the sedimentary rocks. Assuming the constant attenuation coefficients for the anomalies and background, the image reconstruction problem in EG boils down to the problem of finding a binary solution. Using some linear transformations we can assign zero-values to anomalies, and ones to rocks. This assumption is justified since attenuation coefficient of air-filled voids is about zero, but outside the voids

it is rather constant but its value depends on many factors such as parameters of probing signals, lithology and moisture content of the examined medium.

Thus the space of feasible solutions can be narrowed down to the space of discrete points, or even to binary ones. Such harsh constraints can be interpreted in terms of regularization with strong prior information. The binary approach can considerably relax the ambiguities of the least-square inversion, which implies the reduction of the "ghost" effects. For this reason, the usage of image reconstruction algorithms from discrete tomography [25] may be very helpful in solving the image reconstruction problem in EG. Also, such algorithms are much more resistant to noisy perturbations in data, and usually they can be implemented very efficiently.

In our approach, we do not analyze, e.g. stochastic sampling or genetic algorithms that can be also applied for detection of subsurface voids [5].

In the remainder of this paper, a discrete version of EG is referred to as Binary Electromagnetic Geotomography (BEG). The next section briefly describes the model of image reconstruction in BEG. In the third section, some algorithms from binary tomography, which may be useful in our application, are surveyed. We draw particular attenuation to penalized reconstruction with the Markov Random Field (MRF). This section also contains our propositions for adapting well-known algorithms to BEG as well as some hints on their efficient implementation. The numerical results are presented in the fourth section. Finally, the fifth section contains some conclusions.

2. Model

We assume a discrete approximation of the forward projection model, i.e.

$$\sum_{j=1}^{N} \tilde{a}_{ij}\, \tilde{x}_j + n_i = \tilde{b}_i, \quad i = 1, \ldots, M, \tag{1}$$

where M is the number of ray-paths, N is the number of pixels in the image, and usually $M \geq N$, $\tilde{x}_j$ is an attenuation of the j-pixel, $\tilde{a}_{ij}$ is a contribution of the ith ray-path to the jth pixel, n_i is the noisy perturbation of attenuation $\tilde{b}_i$ measured along the ith ray-path. In a matrix notation, we have

$$\tilde{A}\tilde{x} + n = \tilde{b}, \quad \text{where} \quad \tilde{A} \in \mathbb{R}^{M\times N},\ \tilde{x} \in \mathbb{R}^{N},\ n \in \mathbb{R}^{M},\ \tilde{b} \in \mathbb{R}^{M}. \tag{2}$$

To show the motivation for using discrete tomography in our application, first we briefly discuss a classic case of geotomographic image reconstruction. Koltracht et al. [32] proved that for borehole tomography: $\dim \ker(\tilde{A}) \geq n_h$, where n_h is the number of pixels in a horizontal line of the image, and $\ker(\tilde{A})$ is a nullspace of forward projection operator $\tilde{A}$. Assuming the same number of pixels in a vertical line, i.e. $N = n_h^2$, and $M \geq N$, we have $\operatorname{rank}(\tilde{A}) \leq n_h(n_h - 1)$. Our experiments [50] showed that the rank of $\tilde{A}$ is about 91% of N for square matrices. These considerations illustrate a degree of ill-posedness.

Many researches [15,40,42] proposed to apply to geotomography various versions of the ART algorithm [28] that is based on the Kaczmarz algorithm [31]. Tanabe in [58] proved that the limit point of the Kaczmarz algorithm is as follows:

$$\tilde{x}^*(\tilde{x}^{(0)}) = \lim_{k\to\infty} \tilde{x}^{(k)} = P_{\ker(\tilde{A})}\tilde{x}^{(0)} + G\tilde{b}, \tag{3}$$

where $\tilde{x}^{(0)}$ is an initial guess, $P_S(v)$ is an orthogonal projection of v onto subspace S, and $G \in \mathbb{R}^{N\times M}$ is a generalized inversion of $\tilde{A}$. Since $G\tilde{b} \in \ker(\tilde{A})^{\perp}$ (an orthogonal complement of $\ker(\tilde{A})$), this part of x_{true} that falls into the nullspace: $x_{null} = P_{\ker(\tilde{A})}x_{true}$ cannot be reconstructed unless it is included in $\tilde{x}^{(0)}$: $(\tilde{A}x_{null} = 0)$. For noisy data (real data), $\tilde{b} = \tilde{b}_{exact} + \delta\tilde{b} = \tilde{A}\tilde{x}_{true} + \delta\tilde{b}$, where $\delta\tilde{b}$ is a vector of perturbations. For ill-conditioned $\tilde{A}$, $G\delta\tilde{b}$ may even predominate over the minimal-norm least-squares solution of a unperturbed problem: $x_{LS} = G\tilde{b}_{exact}$. For example, let us consider the true image shown in Fig. 2(left), which we then orthogonally project onto $\ker(\tilde{A})^{\perp}$. The projection is illustrated in Fig. 2(right). The vertically smeared structures result from a lack of this part of the true solution that belongs to the nullspace. We usually do not have a sufficient prior knowledge on x_{null}. Thus if $\tilde{x}^{(0)}$ does not include any part of x_{null}, a classic version of the Kaczmarz algorithm cannot give better reconstruction than that presented in Fig. 2(right). Obviously, a degree of smearing artifacts depends on the true image, but for typical geotomographical images (spatially smooth) the artifacts are well visible. In BEG the prior knowledge on possible values of the solution is strongly exploited, which considerably improves the inversion.

To get a binary solution, we transform Eq. (2) to the scaled form:

$$Ax = b, \tag{4}$$

where $x = [x_j]$, $x_j \in \{0, 1\}$, $A = [a_{ij}]$, and $b = [b_i]$ are defined according to the scaling:

- **Multiplicative**: $A = \tilde{A}$, $x = \lambda\tilde{x}$ and $b = \lambda\left(\tilde{b} - n\right)$, where $\lambda = (\xi\bar{x})^{-1}$,
- **Differential**: $A = \tilde{A}$, $x = \bar{x}e - \tilde{x}$ and $b = r - \tilde{b} - n$,

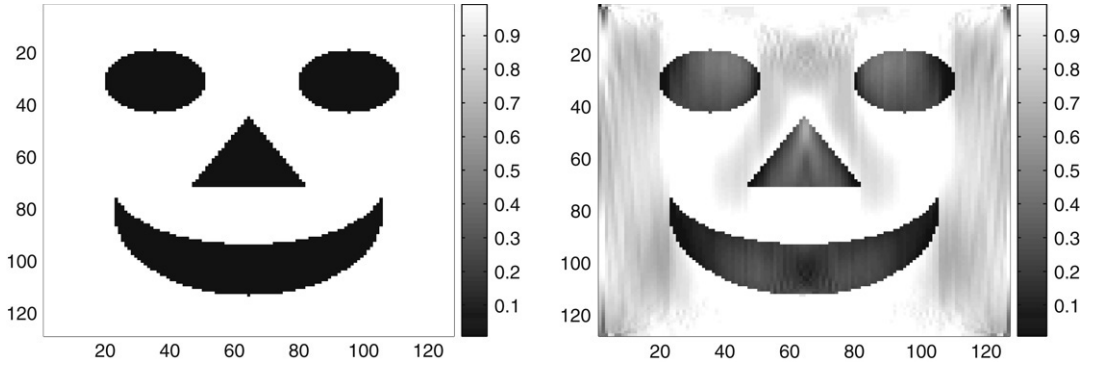

Fig. 2. Phantom image (left); minimal-norm least-squares solution (right).

Table 1
Potential functions

Author(s) (Name)	Functions: $V(u, \delta)$	Reference
Bouman and Sauer (GGMRF)	$\lvert u/\delta\rvert^p$	[7]
Geman and McClure	$\frac{16}{3\sqrt{3}}\frac{(u/\delta)^2}{(1+(u/\delta)^2)}$	[18]
Geman and Reynolds	$\frac{\lvert u/\delta\rvert}{1+\lvert u/\delta\rvert}$	[19]
Green	$\delta \ln[\cosh(u/\delta)]$	[21]
Hebert and Leahy	$\delta \ln\left[1+(u/\delta)^2\right]$	[24]

where $e = [1, \ldots, 1]^{\mathrm{T}} \in \mathbb{R}^N$, $r = [r_i]$, $r_i = \bar{x}\sum_{j=1}^{N} \tilde{a}_{ij}$, and

$$\bar{x} = \frac{\sum_{i=1}^{M} \tilde{b}_i}{\sum_{i=1}^{M}\sum_{j=1}^{N} \tilde{a}_{ij}}$$

is the mean of the attenuation coefficient in the examined medium. In the experiments, we assume about 10% of zero-value pixels in the image, thus $\xi \cong 1.1$. As the perturbations are unknown in real applications, we dropped n, which obviously leads to a system of inconsistent linear equations.

3. Methods

The task of finding the solution to (4) can be expressed in terms of many optimization problems such as Linear Programming (LP) [1,17], Best Inner Fit (BIF) [23,60,61], Non-Linear Integer Programming (NLIP), or Non-Linear Relaxed Programming (NLRP) [55].

We assume that the binary images in BEG contain locally smooth "focused" features which might be well modeled with the MRF model that determines relationships between adjacent pixels. The prior knowledge on the local smoothness can be readily incorporated to an objective function as a regularization term, and hence NLIP and NLRP are more flexible and useful in our application.

For both problems NLIP and NLRP, we define an objective function in terms of the regularized least-squares function:

$$F(x) = ||Ax - b||_2^2 + \beta \sum_{j=1}^{N} \sum_{n\in N_j} w_{jn} V(x_j - x_n, \delta), \tag{5}$$

where the regularization term is formulated with the MRF, and hence, w_{jn} is a weighting factor, N_j is a set of pixels' indices from the nearest neighborhood of pixel j, $V(x_j - x_n, \delta)$ is a clique energy function, β and δ are regularization and scaling parameters.

The clique energy function in (5) attributes, the so-called, "clique energy" to a pair of adjacent pixels. Table 1 lists the functions (in which $u = x_j - x_n$) that are commonly-used in the literature on image processing.

In our experiments, the Generalized Gaussian MRF (GGMRF) function will be denoted by $V^{(BS)}\left(x_j - x_n, p\right)$. This is a scalable function, so δ can be readily merged with the regularization parameter. Its convexity depends on parameter p, but usually $p \in [1, 2]$. For $p = 2$, the function simplifies to the Gaussian one which tends to over-smooth edges of sharp objects, but for $p = 1$ we get the Besag (Laplacian) function [4] that tends to enforce sparse objects. In BEG the objects to

be reconstructed are expected to be large clusters, which justifies the usage of Gaussian models. Moreover, if the objective function is convex, the classic methods for minimizing quadratic objectives can be applied.

On the other hand, the Green function [21], which is referred to as $V^{(GR)}(x_j - x_n, \delta)$, is regarded as more robust, especially as it satisfies all the properties mentioned in [41]. It is non-negative, even, 0 at $u = 0$, strictly increasing for $u > 0$, unbounded, convex, and has bounded first-derivative, so we decided to select this function to our tests.

The above-mentioned problems can be solved with many methods, e.g. trust-region methods for nonlinear minimization (PCG, quasi-Newton methods) [6,14], stochastic sampling (Metropolis–Hasting or Gibbs sampling) [12,43], pattern search methods (Poll method), large-scale primal-dual interior-point methods (e.g. [44]), or D.C. algorithm [47] with convex-concave regularization [55,56]. However, our further considerations are restricted only to specific binary image reconstruction methods that are particular useful when an angular range of projections is very limited. Note that in BEG the limitation is in an angular range of projections (no perpendicular projections) but not in a number of projections as it is usually assumed in many binary tomography algorithms (especially in medical applications of binary tomography) [25,26]. Due to this reason, many well-known binary image reconstruction algorithms for typical applications of binary tomography [27,33–39] cannot be used here.

3.1. Mean-field annealing

The algorithm presented here solves a NLIP problem that is expressed in terms of the regularized least-squares problem: $\min_{x\in\{0,1\}^N} F(x)$ subject to binary constraints. Since the problem of finding a binary solution to the NLIP is non-convex, we use the Mean-Field Annealing (MFA) that iteratively maximizes the Gibbs–Boltzmann distribution

$$P_F(x) = \frac{\exp\{-\frac{F(x)}{T}\}}{\sum\limits_{x\in\{0,1\}^N} \exp\{-\frac{F(x)}{T}\}} \tag{6}$$

which is associated with the objective function $F(x)$ in (5). The ascent towards the global maximum of $P_F(x)$ is controlled with the temperature parameter T.

Theorem 1. *Let x^* be the global maximizer of the Gibbs–Boltzmann distribution (6), then*

$$\lim_{T\to 0} \langle x\rangle_{P_F} \to x^*,$$

where $\langle x\rangle_{P_F}$ means the expectation of x with respect to P_F.

The proof for Theorem 1 can be found, e.g. in [49,62].

Using a Mean-Field (MF) approximation to (6), and applying Theorem 1, the jth pixel value at temperature T can be approximated by the formula:

$$\begin{aligned} x_j(T) &= \frac{\sum\limits_{x_j\in\{0,1\}} x_j \exp\{-\frac{1}{T}F(x_j)\}}{\sum\limits_{x_j\in\{0,1\}} \exp\{-\frac{1}{T}F(x_j)\}} \\ &= \left(1 + \exp\left\{\frac{F(x_j=1) - F(x_j=0)}{T}\right\}\right)^{-1}. \end{aligned} \tag{7}$$

This algorithm was presented in [49], however, our approach concerns a different implementation of this algorithm. Assuming the residual vector $r = Ax - b$ and denoting the jth column vector of A by a_j, then replacing x_j with a zero-value, we can easily update the whole residual vector as follows: $r_0 = r + a_j x_j$. Analogically, we have for $x_j = 1$: $r_1 = r - a_j(1 - x_j)$. Thus $\forall x_j$ the expression $F(x_j = 1) - F(x_j = 0)$ in (7) can be calculated as $||r_1||_2 - ||r_0||_2 + 2\beta\Delta U_j$, where $\Delta U = \sum_{j=1}^{N} \sum_{n\in N_j} w_{jn}\Delta V(x_n, \delta)$ with

$$\Delta V_j^{(GR)}(x_n, \delta) = \delta \ln\left(\frac{1 + \nu\exp\{\frac{2x_n}{\delta}\}}{1 + \exp\{\frac{2x_n}{\delta}\}}\right) - 1, \quad \text{where } \nu = \exp\left\{\frac{2}{\delta}\right\}, \tag{8}$$

$$\Delta V_j^{(BS)}(x_n, p) = |x_n|^p - |1 - x_n|^p, \tag{9}$$

for the clique energy functions $V^{(GR)}(x_n, \delta)$ and $V^{(BS)}(x_n, p)$, respectively. Moreover, after calculating the current approximation for x_j, the whole residual vector can be also similarly updated as $r \leftarrow r - a_j\left(x_j - x_j^{(old)}\right)$. Under the assumption that a_j is very sparse, we need to update for r only a small number of its entries for each j, which considerably accelerates the computations.

(Algorithm MFA)

Initialization Choose $T_0, K_c, \beta, \delta, x^{(0)} = \frac{1}{2}e$,

Outer loop: **For** $s = 0, 1, \ldots,$ **do**

$T^{(s)} = T_0 \exp\left\{-\frac{s}{K_c}\right\}, r \leftarrow b - Ax^{(s)}$,

$x^{(old)} \leftarrow x^{(s)}$,

Inner loop: **For** $j = 0, 1, \ldots, N,$ **do**

$\Delta U_j = \sum_{n\in N_j} w_{jn}\Delta V_j(x_n, \delta)$,

$r_0 \leftarrow r + a_j x_j^{(old)}, r_1 \leftarrow r - a_j\left(1 - x_j^{(old)}\right)$,

$x_j^{(s)} = \left(1 + \exp\left\{\frac{1}{2T^{(s)}}\left(||r_1||_2 - ||r_0||_2 + 2\beta\Delta U_j\right)\right\}\right)^{-1}$,

$r \leftarrow r - a_j\left(x_j^{(s)} - x_j^{(old)}\right)$,

Inner loop: **End**

$x^{(s+1)} \leftarrow x^{(s)}$,

Outer loop: **End**.

Hypothetically, assuming $\forall j$ all a_{ij} are involved in updating r, the computational cost for this algorithm with the Green function is about

$$c^{(GR)} \simeq S\left[(5N^2)_{m/d} + (5N^2)_{a/s} + (MN)_{m/d} + (MN)_{a/s} + (43N)_{m/d} + (27N)_{a/s} + (16N)_f\right],$$

where the subscripts m, d, a, s, and f denote the elementary multiplication, division, addition, subtraction, and function evaluation operation, respectively. For the function $V^{(BS)}(x_n, p)$ the cost decreases by $S\left((8N)_{m/d} + (8N)_{a/s}\right)$.

3.2. Binary steering of projected gradient algorithm

The method proposed here is based on the Projected Gradient (PG) method [3] that finds a stationary point $x^* \in X \subseteq \mathbb{R}^N$ to the problem:

$$x^* = \arg\min_x F(x), \quad \text{s.t.} \quad x \in X, \tag{10}$$

with the following iterative formula:

$$x^{(k+1)} = P[x^{(k)} - \alpha^{(k)}\nabla_x F(x)|_{x=x^{(k)}}], \quad \text{for } k = 0, 1, \ldots, \tag{11}$$

where X is a non-empty, closed and convex set of feasible solutions, and $P[\xi]$ is a projection of ξ onto X. The stationarity is reached when $x^* = P[x^* - \nabla_x F(x)|_{x=x^*}]$. The convergence of the PG method was proved, e.g. in [9,30].

In our approach, we assumed that

$$P[\xi^{(k)}] = \begin{cases} 0 & \text{if } \xi^{(k)} \le \eta^{(k)}, \\ 1 & \text{if } \xi^{(k)} \ge 1 - \eta^{(k)}, \\ \xi^{(k)} & \text{otherwise.} \end{cases} \tag{12}$$

This choice was motivated by the binary steering technique proposed in [11]. Following the temperature schedule as in the MFA algorithm, we propose to iteratively shrink the bound constraints $[\eta^{(k)}, 1 - \eta^{(k)}]$ according to the exponentiated rule:

$$\eta^{(k)} = \frac{1}{2}\left(1 - \exp\left\{-\frac{k}{\delta}\right\}\right), \tag{13}$$

where $\delta > 1$ is a constant that controls a speed of convergence towards a binary solution. When $k << \delta$, the algorithm solves a NLRP problem, and an increase in a number of iterations gradually steers the iterative updates towards binary values. For $k >> \delta$, the algorithm solves a NLIP problem. Similarly as in the MFA, the descent towards a binary solution cannot be too steep because the iterative process can stuck in local minima. The parameter δ should be therefore carefully selected. Our experiments showed that the reconstruction is not very sensitive to $\delta \in [10, 500]$.

In general, gradient algorithms are regarded as slow methods, however, their convergence rate strongly depends on the step length $\alpha^{(k)} \in (0, 1]$ in (11). There are many rules for choosing $\alpha^{(k)}$, but we restrict our considerations only to the inexact line search that is known as the "Armijo rule along a projection arc" [3]. The step length is optimal if

$$\alpha^{(k)} = \beta^{m_k}, \tag{14}$$

where m_k is the first non-negative integer m for which

$$F(x^{(k+1)}) - F(x^{(k)}) \le \sigma\nabla F(x^{(k)})^T(x^{(k+1)} - x^{(k)}), \tag{15}$$

for $\sigma \in (0, 1)$. In our algorithm, we selected $\beta = 0.5, \sigma = 0.001$.

(Binary Steering of Projected Gradient Algorithm (BS-PG))

Initialization: Set $\beta,\ \delta,\ \tau,\ \tau_f,\ \sigma,\ \epsilon,\ \alpha_{\min},\ e=[1,\ldots,1]^T\in\mathbb{R}^N$,
$b\leftarrow Ae-b,\ x^{(0)}=\frac{1}{2}e,\ \tau_g=||A^Tb||_2\,\tau$,

Outer loop: **For** $k=0,1,\ldots,$ **do**
$\eta^{(k)}=\frac{1}{2}\left(1-\exp\left\{-\frac{k}{\delta}\right\}\right)$,
$Z^{(k)}=\left\{j\in\{1,\ldots,N\}:|x_j^{(k)}|>\epsilon\right\}$,
$A_s^{(k)}=[a_{*,Z^{(k)}}],\ L_s^{(k)}=[l_{*,Z^{(k)}}],\ x_s^{(k)}=[x_{Z^{(k)}}^{(k)}]$,
$r\leftarrow b-A_s^{(k)}x_s^{(k)},\ q\leftarrow L_s^{(k)}x_s^{(k)}$,
$\phi=-A^Tr,\ \psi=L^Tq$,
$f\leftarrow\frac{1}{2}r^Tr+\frac{1}{2}\beta q^Tq$,
$g\leftarrow\phi+\beta\psi$,
$Z_g^{(k)}=\left\{j\in\{1,\ldots,N\}:g_j<0\right\}$,

Termination: **If** $||g_{Z_g^{(k)}}||_2<\tau_g$,
Break
End
$\alpha=1$,

Inner loop: **While** $\alpha>\alpha_{\min}$ **do**
$\alpha\leftarrow\frac{\alpha}{2},\bar{x}\leftarrow x-\alpha g$,

$$\hat{x}\leftarrow\begin{cases}0 & \text{if} \quad \bar{x}\le\eta^{(k)},\\ 1 & \text{if} \quad \bar{x}\ge 1-\eta^{(k)},\\ \bar{x} & \text{otherwise}\end{cases}$$

$\hat{r}\leftarrow b-A\hat{x},\ \hat{q}\leftarrow L\hat{x}$,
$\hat{f}\leftarrow\frac{1}{2}\hat{r}^T\hat{r}+\frac{1}{2}\beta\hat{q}^T\hat{q}$,

Termination: **If** $\hat{f}-f\le\sigma g^T(\hat{x}-x)$: $x^{(k+1)}=\hat{x}$,
Break
End

Inner loop: **End**
$x^{(k+1)}=\hat{x}$,

Termination: **If** $k>1$ and $\frac{x^T(1-x)}{N}<\tau_f$: $x^{(k)}\leftarrow 1-x^{(k)}$.
Break
End

Outer loop: **End**

On the contrary to the MFA algorithm, the BS-PG algorithm updates all the entries in x simultaneously, and to avoid the inner loop, we apply only the GGMRF function for $p=2$. For this case and under the assumption of the first-order interactions between pixels (only along vertical and horizontal lines), the objective function in (5) can be simplified to the quadratic function:

$$F(x)=||b-Ax||_2^2+\beta||Lx||_2^2, \tag{16}$$

where $L=I-W/4, I\in\mathbb{R}^{N\times N}$ is an identity matrix, $W=[w_{jn}]$,

$$w_{jn}=\begin{cases}1, & \text{for } \forall n\in\{j-n_h,j-1,j+1,j+n_h\},\\ 0, & \text{otherwise},\end{cases} \tag{17}$$

is the weighting matrix, and n_h is the number of pixels in a horizontal line.

Since matrix–vector multiplications: Ax and Lx must be executed many times, we avoid computing on the whole size of the matrices. In BEG, the images to be reconstructed are expected to have only a few clusters of zero-value pixels, and the background represented by unit-value pixels, hence, we introduce the following transformation:

$$b\leftarrow Ae-b,\quad \text{where } e=[1,\ldots,\ 1]^{\mathrm{T}}\in\mathbb{R}^N, \tag{18}$$

and after the termination of the algorithm, the back-transformation is applied: $x\leftarrow 1-x$. In this way, only a few entries of the vector x have unit-values. To decrease an overall computational cost substantially the columns in A and L that correspond to zero-value entries in x are removed at each iteration k. This procedure is motivated by the active set methods widely known in the optimization theory. Thus, the number of arithmetic operations changes in each iteration, and cannot be easily estimated. Thus, the computational complexity is estimated with the elapsed time (from the initialization to the assumed termination).

This algorithm is terminated where one of the stop criteria: $||\nabla F(x^{(k)})||_2<\tau_g$ or $(x^{(k)})^{\mathrm{T}}(1-x^{(k)})<N\tau_f$ is met. We set $\tau_g=||A^Tb||_2\,\tau$ with $\tau=10^{-4}$, $\tau_f=5\times10^{-4}$, $\alpha_{\min}=10^{-12}$, and $\epsilon=10^{-16}$.

4. Results

The results are assessed by means of the quality and quantity criteria. The former concerns displaying the solution on a 2D patch plot. The latter is the average distance measure that was introduced in [10].

The synthetic data are generated from the binary phantom image (with resolution 128 × 128 pixels) that is shown in Fig. 2(left). In real case, the image to be reconstructed is expected to have some clusters of zero-value pixels. The shape of these objects should be in most cases ellipsoidal due to diffraction and refraction of electromagnetic waves around strong inhomogeneities. However, other *non-convex* objects may also occur. Thus, we cannot assume the compact object reconstruction as in [45].

Let us assume that each pixel is a square of 1 × 1 m. The original images are associated with a typical electromagnetic geotomographic area that is probed along multiple straight-line rays traced between transmitter points regularly spaced along one borehole and receiver points regularly spaced along the other borehole. Thus, there is one transmitter/receiver point in each pixel adjacent to a borehole.

The noisy data are obtained by adding a zero-mean Gaussian noise to the noise-free data. The variance of the noise is adjusted to have a target Signal-to-Noise Ratio (SNR) that is computed according to the definition:

$$SNR \triangleq 20 \log \frac{||\tilde{b}_{exact}||_2}{||n||_2}, \quad \text{dB} \tag{19}$$

where $\tilde{b}$ and n are given by (2). We used the noisy data for which $SNR = 20$ dB. The noise level was estimated from our real data, using the technique given in [52]. Typically, 5% noise level (about 26 dB) is regarded in EG simulations [15,40,52], but we assume a little bit more noisy data due to the neglect of the wave scattering effects.

The results obtained with the MFA, BS-PG, and ART algorithms are shown in Figs. 3–6. The MFA algorithm has been run with various clique energy functions and the associated parameters (β, δ, and p), but we present the results only for the $V_j^{(GR)}$ and $V_j^{(BS)}$. The results obtained for other clique energy functions are slightly worse than that for $V_j^{(GR)}$. In the BS-PG algorithm, we applied only the Gaussian prior since only for this case the computational cost is very low.

All the discussed algorithms were implemented in Matlab 7.0 and the computational cost is roughly estimated in terms of the elapsed time which amounts to 9.56, 0.96, and 424.15 s per one iteration (cycle in the ART) for the MFA, BS-PG, and ART algorithms, respectively.

The parameters T_0 and K_c which set the temperature schedule are nearly the same as in [62]. They are adjusted experimentally, but in general, higher values of the parameters always improve the quality of the reconstruction but at the cost of a convergence rate. In general, there are many heuristics for determining the temperature schedule — one of them assumes that the temperature should not decrease faster than $T(k) = \frac{T_0}{\ln k}$ [29,13,18].

The scaling parameter in $V_j^{(GR)}$ is roughly estimated as $\delta = 0.01$ using the Maximum Likelihood (ML) approach proposed in [54]. The estimation of β can be efficiently done with marginalization, i.e. maximization of Type II likelihood [20]. Another option for doing this is to apply the tools such as Generalized Cross-Validation (GCV), L-curve [6] (especially for BS-PG), or even the ML estimate presented in [54].

The synthetic results obtained with the MFA algorithm (Figs. 3–5) are surprisingly good. For noise-free data nearly all the clique energy functions give satisfactory results (see Fig. 4). For noisy data the best reconstruction is obtained with the Green function (see Fig. 3). For the GGMRF model, the results strongly depend on p. If this parameter is close to its lower bound ($p = 1$), the reconstructed image is speckled with noise. This is because the Besag function enforces sparse objects, and this case should be avoided for very noisy BEG data, even if some sparse objects are expected to be reconstructed. For $p = 2$, we observe the over-smoothing, and such a case is also unacceptable.

The good results are also obtained with BS-PG algorithm. In spite of applying only the Gaussian prior that is an equivalent to the GGMRF model, the over-smoothing is not visible in the images reconstructed from noisy data (see Fig. 3). We decided to use the Gaussian prior only due to the computational cost. For the regularization term with the Green function, the results would be presumably much better.

For comparison, we also used a classic version of the ART algorithm [28]. For noise-free data, the relaxation parameter is set as $\omega = 1$. The image reconstructed after 100 iterations, which is shown in Fig. 3 (fourth left row), is nearly the same as the projection results given in Fig. 2(right). A further increase in the number of iterations does not affect this result significantly. For noisy data, a lower value of the parameter must be set, i.e. $\omega = 0.05$ (according to the hints in [52]). For $k = 5$, we get the image with the lowest value of the distance. For $k > 5$, the result worsens (see Fig. 3 (fourth right row)).

Additionally, we applied the discussed algorithms to the preliminary real data that was measured in Myslovice (Upper Silesia in Poland). The area at a depth ranging from 50 m to 65 m was probed with a wave at the single frequency 2 MHz. All the reconstruction results given in Fig. 6 demonstrate that the area is strongly inhomogeneous, and the images are consistent at some degree. But only the binary algorithms provide extensive information on positions and shapes of the air-filled voids. Probably, the small voids adjacent to the boreholes can be considered as artifacts. The shape of the inhomogeneous objects is rather oblong but this is mostly caused by the very low resolution of the images due to a severely limited number of probings.

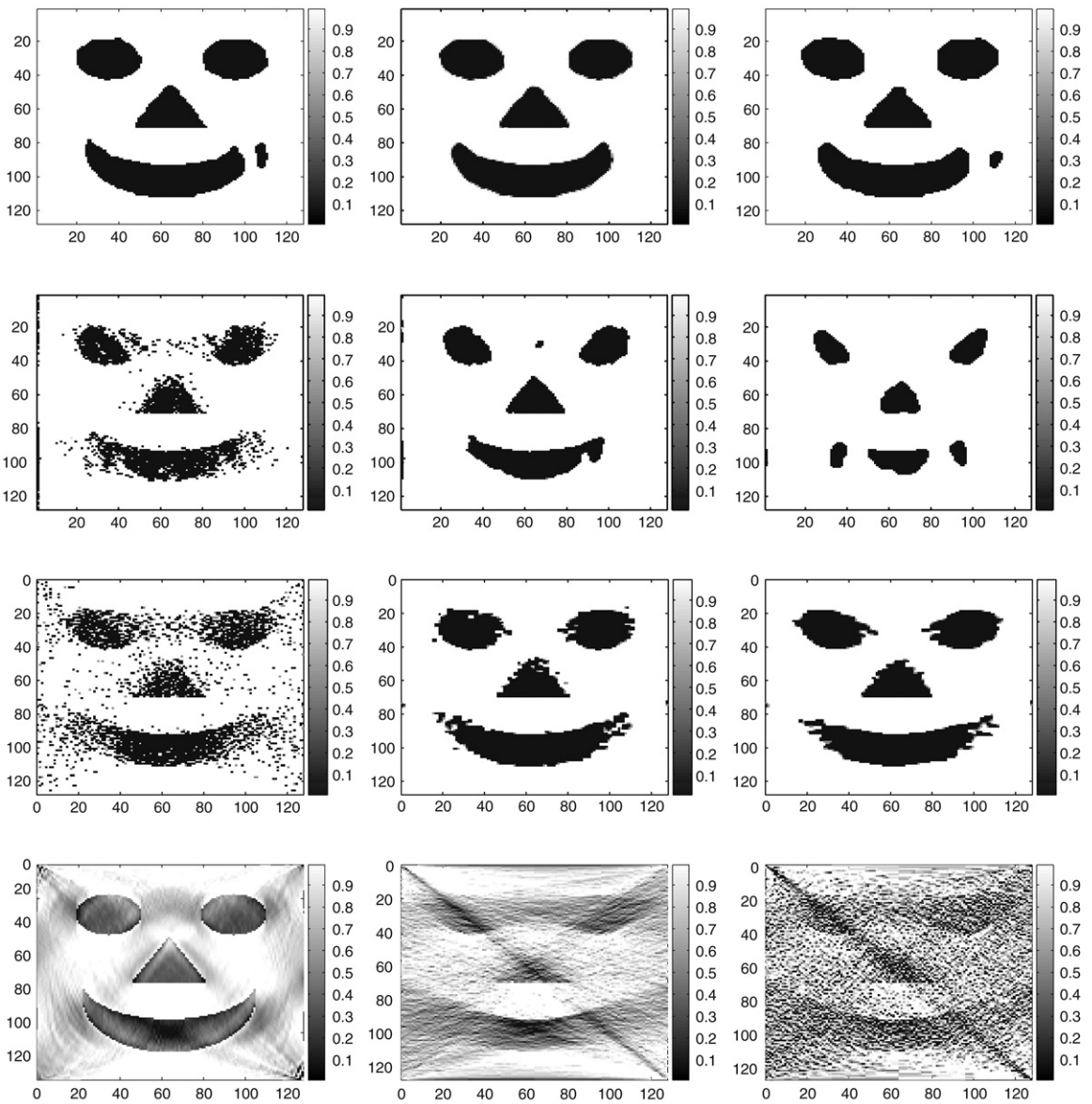

Fig. 3. Images reconstructed with the following algorithms: (first (top) row) MFA from noisy data for $k = 300$, $K_c = 40$, $T_0 = 0.5$, $\Delta V_j^{(GR)}(\delta = 0.01)$: $\beta = 0.05$ (left), $\beta = 0.1$ (middle), $\beta = 0.3$ (right); (second row) MFA from noisy data for $k = 300$, $K_c = 40$, $T_0 = 0.5$, $\Delta V_j^{(BS)}$, $\beta = 0.05$: $p = 1.1$ (left), $p = 1.5$ (middle), $p = 1.9$ (right); (third row) BS-PG from noisy data for $k = 300$, $\delta = 100$: $\beta = 50$ (left), $\beta = 1000$ (middle), $\beta = 5000$ (right); (fourth row) ART: noise-free data, $k = 100, \omega = 1$ (left), noisy data, $k = 5, \omega = 0.05$ (middle), noisy data, $k = 20, \omega = 0.05$ (right). Noise level set as $SNR = 20$ dB.

5. Conclusions

In this paper, the selected binary image reconstruction algorithms are discussed in the context of their application to a discrete version of electromagnetic geotomography which we denote as BEG. We discuss many aspects related to BEG. Regarding the algorithmic approach, we propose a new very efficient implementation of the MFA algorithm [49] and the BS-PG algorithm. The algorithms iteratively minimize the MRF regularized least-squares objective function subject to binary constraints. Although many other algorithms for binary tomography exist, the discussed algorithms are particularly efficient when BEG is considered. This is confirmed by the numerical experiments in which we use synthetic and real data. The MFA, BS-PG, and additionally ART algorithms are compared with respect to multi-criteria performance such as reconstruction exactness, robustness to noisy perturbations, as well as computational complexity. On the whole, the MFA with the Green function in the MRF model is the most robust to very noisy data. However, one must be aware of the fact that the high performance is parameter-dependant. The associated parameters can be estimated prior to the reconstruction, but it involves additional, quite a large computational cost. The GGMRF is more flexible in application to the discussed algorithms,

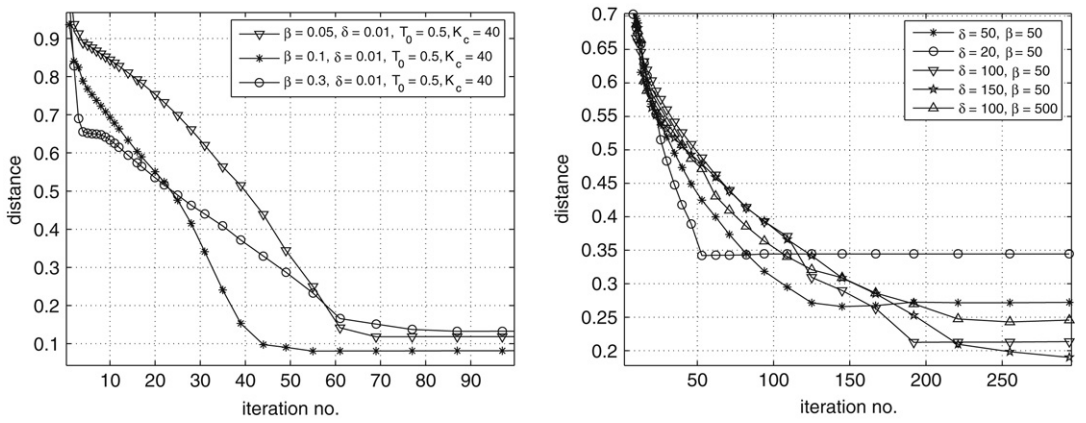

Fig. 4. Distances between x_{exact} and the reconstructed solution obtained from noise-free data with the algorithms: (left) MFA for $K_c = 40$, $T_0 = 0.5$, $\Delta V_j^{(GR)}(\delta = 0.01)$; (right) BS-PG.

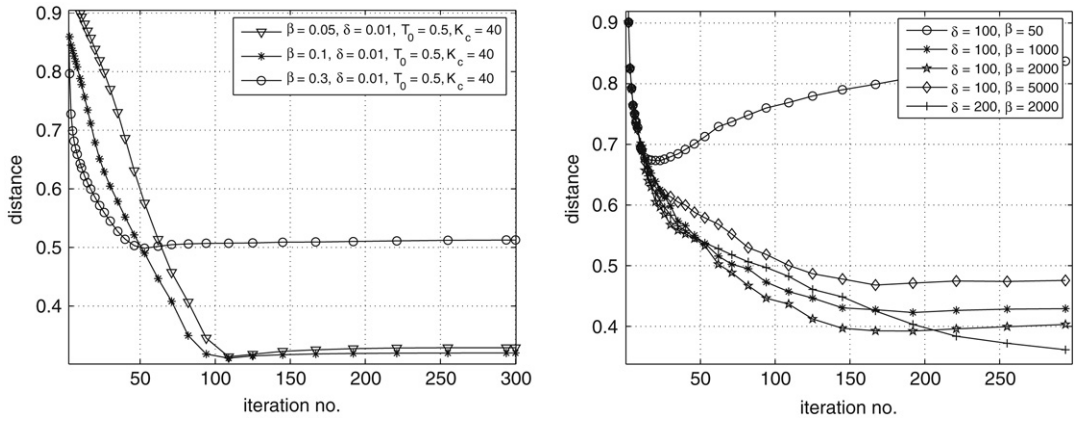

Fig. 5. Distances between x_{exact} and the reconstructed solution obtained from noisy data ($SNR = 20$ dB) with the algorithms: (left) MFA for $K_c = 40$, $T_0 = 0.5$, $\Delta V_j^{(GR)}(\delta = 0.01)$; (right) BS-PG.

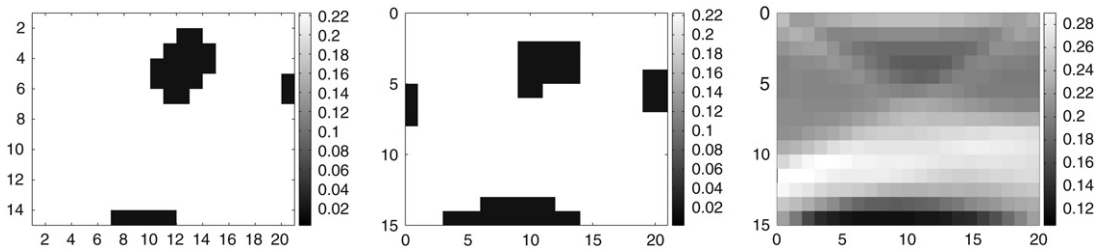

Fig. 6. Images reconstructed from real data with the algorithms: (left) MFA for $k = 300$, $K_c = 40$, $T_0 = 0.5$, $\Delta V_j^{(GR)}(\delta = 0.01)$, $\beta = 0.1$; (middle) BS-PG for $k = 300$, $\delta = 100$, $\beta = 500$; (right) ART for $k = 5$, $\omega = 0.05$.

especially in the BS-PG. Although the quality of the images reconstructed with the BS-PG is not so high as with the MFA involving the Green function, the BS-PG is about 10 times faster than the MFA. Thus the BS-PG seems to be more suitable for solving very large-scale BEG problems.

Acknowledgments

The author would like to thank Prof. Andrzej Pralat, Institute of Telecommunications, Teleinformatics and Acoustics, Wroclaw University of Technology, Poland, for providing the real data from EG. The author is also grateful to the anonymous reviewers for their valuable comments and suggestions.

References

[1] R. Aharoni, G.T Herman, A. Kuba, Binary vectors partially determined by linear equation systems, Discrete Math. 171 (1997) 1–16.

[2] A. Becht, J. Tronicke, E. Appel, P. Dietrich, Inversion strategy in crosshole radar tomography using information of data subsets, Geophysics 69 (2004) 222–230.
[3] D.P. Bertsekas, On the Goldstein–Levitin–Polyak gradient projection method, IEEE Trans. Automat. Control 21 (1976) 174–184.
[4] J. Besag, Toward Bayesian image analysis, J. Appl. Stat. 16 (1989) 395–407.
[5] R.S. Bichkar, S.K. Singh, A.K. Ray, Genetic algorithmic approach to detection of subsurface voids in cross-hole seismic tomography, Pattern Recognit. Lett. 19 (1998) 527–536.
[6] A. Björck, Numerical Methods for Least Squares Problems, SIAM, Philadelphia, 1996.
[7] C.A. Bouman, K. Sauer, A generalized Gaussian image model for edge-preserving map estimation, IEEE Trans. Image Process. 2 (1993) 296–310.
[8] N.D. Bregman, R.C. Bailey, C.H. Chapman, Ghosts in tomography: The effect of poor angular coverage in 2-D seismic traveltime inversion, Can. J. Expl. Geophys. 25 (1989) 7–27.
[9] P.H. Calamai, J.J. More, Projected gradient methods for linearly constrained problems, Math. Program. 39 (1987) 93–116.
[10] Y. Censor, D. Gordon, R. Gordon, Component averaging: An efficient iterative parallel algorithm for large and sparse unstructured problems, Parallel Comput. 27 (2001) 777–808.
[11] Y. Censor, S. Matej, Binary steering of nonbinary iterative algorithms, in: G.T. Herman, A. Kuba (Eds.), Discrete Tomography: Foundations, Algorithms, and Applications, Springer, New York, 1999, pp. 285–296.
[12] M.T. Chan, G.T. Herman, E. Levitan, Bayesian image reconstruction using image-modeling Gibbs priors, Int. J. Imaging Syst. Technol. 9 (1998) 85–98.
[13] D. Chandler, Introduction to Modern Statistical Mechanics, Oxford Univ. Press, Oxford, U.K, 1987.
[14] T.F. Coleman, Y. Li, An interior, trust region approach for nonlinear minimization subject to bounds, SIAM J. Optim. 6 (1996) 418–445.
[15] K.A. Dines, R.J. Lytle, Computerized geophysical tomography, Proc. IEEE 67 (1979) 1065–1073.
[16] B. Dyer, M.H. Worthington, Some sources of distortion in tomographic velocity images, Geophys. Prospect 36 (1988) 209–222.
[17] P. Fishburn, P. Schwander, L. Shepp, R. Vanderbei, The discrete Radon transform and its approximate inversion via linear programming, Discrete Appl. Math. 75 (1997) 39–61.
[18] S. Geman, D. McClure, Statistical methods for tomographic image reconstruction, Bull. Int. Stat. Inst. LII-4 (1987) 5–21.
[19] S. Geman, G. Reynolds, Constrained parameters and the recovery of discontinuities, IEEE Trans. Pattern Anal. Mach. Intell. 14 (1992) 367–383.
[20] I.J. Good, The Estimation of Probabilities: An Essay on Modern Bayesian Methods, MIT Press, Cambridge, MA, 1965.
[21] P.J. Green, Bayesian reconstruction from emission tomography data using a modified EM algorithm, IEEE Trans. Med. Imaging 9 (1990) 84–93.
[22] R. Gritto, Subsurface void detection using seismic tomographic imaging, LBNL-53227, Lawrence Berkeley National Laboratory, Berkeley, USA, 2003.
[23] P. Gritzmann, S. de Vries, M. Wiegelmann, Approximating binary images from discrete X-rays, SIAM J. Optim. 11 (2000) 522–546.
[24] T. Hebert, R. Leahy, A generalized EM algorithm for 3-D Bayesian reconstruction form Poisson data using Gibbs priors, IEEE Trans. Med. Imaging 8 (1989) 194–202.
[25] G.T. Herman, A. Kuba (Eds.), Discrete Tomography: Foundations, Algorithms, and Applications, Birkhauser, Boston, 1999.
[26] G.T. Herman, A. Kuba (Eds.), Advances in Discrete Tomography and Its Applications, Birkhauser, Boston, 2007.
[27] G.T Herman, A. Kuba, Discrete tomography in medical imaging, Proc. IEEE 91 (2003) 1612–1626.
[28] G.T. Herman, A. Lent, S. Rowland, ART: Mathematics and applications (a report on the mathematical foundations and on the applicability to real data of the algebraic reconstruction techniques), J. Theoret. Biol. 42 (1973) 1–32.
[29] L. Ingber, Simulated annealing: Practice versus theory, J. Math. Comput. Modelling 18 (1993) 29–57.
[30] A.N. Iusem, On the convergence properties of the projected gradient method for convex optimization, Comput. Appl. Math. 22 (2003) 37–52.
[31] S. Kaczmarz, Angenaherte auflosung von systemem linearer gleichungen, Bull. Acad. Pol. Sci. Lett. 35 (1937) 355–357.
[32] I. Koltracht, P. Lancaster, D. Smith, The structure of some matrices arising in tomography, Linear Algebra Appl. 130 (1990) 193–218.
[33] A. Kuba, Reconstruction of two-directionally connected binary patterns from their two orthogonal projections, Computer Vis. Graph. Image Process. 27 (1984) 249–265.
[34] A. Kuba, E. Balogh, Reconstruction of convex 2D discrete sets in polynomial time, Theoret. Comput. Sci. 283 (2002) 223–242.
[35] A. Kuba, G.T. Herman, S. Matej, A. Todd-Pokropek, Medical applications of discrete tomography, in: Discrete Mathematical Problems in Medical Applications, in: Ser. DIMACS Series in Discrete Mathematics and Theoretical Computer Science, vol. 55, AMS, 2000, pp. 195–208.
[36] A. Kuba, A. Nagy, E. Balogh, Reconstruction of hv-convex binary matrices from their absorbed projections, Discrete Appl. Math. 139 (2004) 137–148.
[37] A. Kuba, M. Nivat, Reconstruction of discrete sets with absorption, Linear Algebra Appl. 339 (2001) 171–194.
[38] A. Kuba, M. Nivat, A sufficient condition for non-uniqueness in binary tomography with absorption, Theoret. Comput. Sci. 346 (2005) 335–357.
[39] A. Kuba, L. Rusko, L. Rodek, Z. Kiss, Preliminary studies of discrete tomography in neutron imaging, IEEE Trans. Nucl. Sci. 52 (2005) 380–385.
[40] D.L. Lager, R.J. Lytle, Determining a subsurface electromagnetic profile from high frequency measurements by applying reconstruction technique algorithms, Radio Sci. 12 (1977) 249–260.
[41] K. Lange, Convergence of EM image reconstruction algorithms with Gibbs smoothing, IEEE Trans. Med. Imaging 9 (1900) 439–446.
[42] R.J. Lytle, E.F. Laine, D.L. Lager, D.J. Davis, Using cross borehole electromagnetic probing to locate high contrast anomalies, Geophysics 44 (1979) 1667–1676.
[43] S. Matej, G.T. Herman, A. Vardi, Binary tomography on the hexagonal grid using Gibbs priors, Int. J. Image Syst. Technol. 9 (1998) 126–131.
[44] S. Mehrotra, On the implementation of a primal-dual interior point method, SIAM J. Optim. 2 (1992) 575–601.
[45] A. Mohammad-Djafari, C. Soussen, Compact object reconstruction, in: G.T. Herman, A. Kuba (Eds.), Discrete Tomography: Foundations, Algorithms, and Applications, Springer, New York, 1999, pp. 317–342.
[46] M.N. Nabighian (Ed.), Electromagnetic Methods in Applied Geophysics, in: Society of Exploration Geophysicists, vol. 2, Tulsa, 1991.
[47] T. Pham Dinh, L.T. Hoai An, A D.C. optimization algorithm for solving the trust-region subproblem, SIAM J. Optim. 8 (1998) 476–505.
[48] W.S. Phillips, M.C. Fehler, Traveltime tomography: A comparison of popular methods, Geophysics 56 (1991) 1639–1649.
[49] J.W. Phillips, R.M. Leahy, J.C. Mosher, MEG-based imaging of focal neuronal current sources, IEEE Trans. Med. Imaging 16 (1997) 338–348.
[50] C. Popa, R. Zdunek, Kaczmarz extended algorithm for tomographic image reconstruction from limited-data, Math. Comput. Simul. 65 (2004) 579–598.
[51] A. Pralat, R. Zdunek, Electromagnetic geotomography — selection of measuring frequency, IEEE Sensors J. 5 (2005) 242–250.
[52] R.D. Radcliff, C.A. Balanis, Reconstruction algorithms for geophysical applications in noisy environments, Proc. IEEE 67 (1979) 1060–1064.
[53] P.S. Rowbotham, R.G. Pratt, Improved inversion through use of the null space, Geophysics 62 (1997) 869–883.
[54] S.S. Saquib, C.A. Bouman, K. Sauer, ML parameter estimation for Markov random fields with applications to Bayesian tomography, IEEE Trans. Image Process. 7 (1998) 1029–1044.
[55] T. Schule, C. Schnorr, S. Weber, J. Hornegger, Discrete tomography by convex-concave regularization and D.C. programming, Discrete Appl. Math. 151 (2005) 229–243.
[56] T. Schule, S. Weber, C. Schnorr, Adaptive reconstruction of discrete-valued objects from few projections, Electron. Notes Discrete Math. 20 (2005) 365–384.
[57] R. Snieder, J. Trampert, Inverse problems in geophysics, in: A. Wirgin (Ed.), Wavefield Inversion, Springer-Verlag, New York, 1999, pp. 119–190.
[58] K. Tanabe, Projection method for solving a singular system of linear equations and its applications, Numer. Math. 17 (1971) 203–214.
[59] A. van der Sluis, H.A. van der Vorst, Numerical solution of large, sparse linear algebraic systems arising from tomographic problems, in: G. Nolet (Ed.), Seismic Tomography with Applications in Global Seismology and Exploration Geophysics, D. Reidel Publ. Co, 1987, pp. 49–83.
[60] S. Weber, C. Schnorr, J. Hornegger, A linear programming relaxation for binary tomography with smoothness priors, in: Proceedings of International Workshop on Combinatorial Image Analysis, IWCIA'03, Palermo, Italy, May 14–16, 2003.
[61] S. Weber, T. Schule, J. Hornegger, C. Schnorr, Binary tomography by iterating linear programs from noisy projections, in: IWCIA 2004, in: LNCS, vol. 3322, 2004, pp. 38–51.
[62] R. Zdunek, A. Pralat, Detection of subsurface bubbles with discrete electromagnetic geotomography, Electron. Notes Discrete Math. 20 (2005) 535–553.